Journal of Alloys and Compounds 504S (2010) S117–S122

Contents lists available at ScienceDirect

Journal of Alloys and Compounds

journal homepage: www.elsevier.com/locate/jallcom

Effect of cooling rate on microstructure and mechanical properties of rapidly solidified Al-based bulk alloys

Longchao Zhuo, Shujie Pang, Hui Wang, Tao Zhang*

Key Laboratory of Aerospace Materials and Performance (Ministry of Education), School of Materials Science and Engineering, Beijing University of Aeronautics and Astronautics, Beijing 100191, China

ARTICLE INFO

Article history:
Received 1 November 2009
Received in revised form 11 March 2010
Accepted 26 March 2010
Available online 2 April 2010

Keywords:
Amorphous materials
Rapid-solidification
Microstructure
Mechanical properties

ABSTRACT

The microstructure and mechanical properties of $Al_{86}Si_{0.5}Ni_{4.06}Co_{2.94}Y_6Sc_{0.5}$ alloys produced by copper mold casting at different cooling rates were investigated. With decreasing the cooling rate during solidification, the microstructure for these rapidly solidified alloys varied from almost fully amorphous for 1-mm-diameter rod to chill-zone surface layered structures for 1.5-mm- and 2-mm-diameter ones. Compared to the 1-mm-diameter alloy rod formed at a faster cooling rate, the 1.5-mm- and 2-mm-diameter alloys possess lower strength, whereas larger compressive plasticity due to the formation of composite structure with soft inner core and hard chill-zone outer shell. The results indicate that the mechanical properties of the rapidly solidified Al-based bulk alloys can be tunable by employing proper cooling rate.

1. Introduction

The development of advanced light-weight Al-based alloys is consistently focused on meeting new requirements in various application fields such as for transportation systems and energy consumption [1–4]. As a new type and an intriguing class of potential advanced structural materials, Al-based alloys in amorphous state, firstly developed 20 years ago [5,6], are attractive owing to their unique combination of high strength and ductility, as well as low density, low elastic modulus and good corrosion resistance [7]. Partially or completely crystallized versions of these Al-based alloys have been shown to offer promise of even higher strength with ductility when suitable mixtures of nanoscale crystalline, quasicrystalline or amorphous phase exist [8,9]. However, due to their poor glass-forming ability (GFA), the formation of Al-based metallic glasses or the corresponding glass matrix composites is limited to thin ribbons [7,10], and the synthesis of ultrahigh-strength Al-based alloys in bulk form prepared by multi-step powder metallurgy method suffers from porosity and contamination problems [7], which restricts their practical application.

Recently, Al-based alloys with high glass-forming ability, for which the critical diameter for glass formation is 1 mm or approaches 1 mm by copper mold casting, have been reported [11,12]. The cast Al–Si–Ni–Co–Y–Sc rod with a diameter of 1 mm is composed of almost fully amorphous structure besides ~5% fcc-Al and possesses an ultrahigh strength up to 1.27 GPa and plastic strain of ~2.4% in compression [12]. In this work, the Al–Si–Ni–Co–Y–Sc bulk alloys with various diameters, corresponding to different cooling rates during solidification, were prepared by copper mold casting, and the corresponding microstructure, Vickers microhardness as well as compressive mechanical properties were investigated. The effects of cooling rate on the microstructure and mechanical properties of the Al-based bulk alloys have been discussed in detail.

2. Experimental

The master alloys with a nominal composition of $Al_{86}Si_{0.5}Ni_{4.06}Co_{2.94}Y_6Sc_{0.5}$ were prepared by arc melting the pure metals (over 99.9 mass%) in argon atmosphere. The ingots were melted 3–4 times to ensure chemical homogeneity. After mechanically ground to remove surface oxide, the ingots were remelted and then cast into copper molds to obtain cylindrical rods with diameters of 1 mm, 1.5 mm and 2 mm, respectively. The as-cast rods were examined by X-ray diffraction (XRD) using a Bruker AXS D8 X-ray diffractometer with Cu-Kα radiation. The characteristic backscattered images of cross-section of the rods were obtained on JSM-5800 scanning electron microscopy (SEM) equipped with energy dispersive X-ray spectroscopy (EDS).

Compressive tests of the as-cast rods with a height to diameter ratio of 2:1 were carried out on an Instron 5565 testing machine at a strain rate of $5 \times 10^{-4}\ s^{-1}$. Vickers microhardness was measured using 100 g indentation load applied for 10 s. Each microhardness value in the results was the average of 10 individual indents examined in each characteristic structured zone for each sample.

3. Results and discussion

The $Al_{86}Si_{0.5}Ni_{4.06}Co_{2.94}Y_6Sc_{0.5}$ alloy rods with different sizes, i.e. 1 mm, 1.5 mm and 2 mm in diameters, were prepared by copper

* Corresponding author. Tel.: +86 10 82339705; fax: +86 10 82334869.
E-mail address: zhangtao@buaa.edu.cn (T. Zhang).

0925-8388/$ – see front matter © 2010 Elsevier B.V. All rights reserved.
doi:10.1016/j.jallcom.2010.03.211

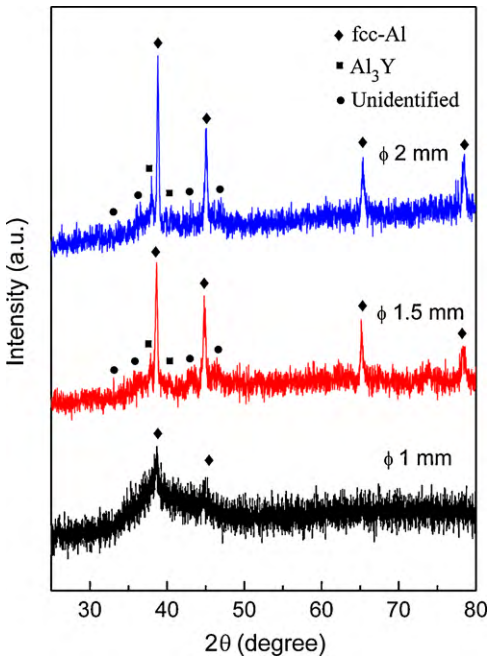

Fig. 1. XRD patterns of $Al_{86}Si_{0.5}Ni_{4.06}Co_{2.94}Y_6Sc_{0.5}$ rods of 1 mm, 1.5 mm and 2 mm in diameters prepared by copper mold casting.

mold casting to investigate the dependence of the microstructure and mechanical properties on cooling rate (R_c). R_c of the samples can be estimated according to $R_c = 0.4K_tT_l/C_pL^2$ [13], where K_t is the thermal conductivity, C_p is the specific heat, T_l is the melting temperature, and L is the critical thickness of the plate. Here we take $K_t \sim 0.1$ W/cm s^{-1} K^{-1}, $C_p \sim 4$ J/cm^3 K^{-1} (typical of a molten alloy) and $T_l \sim 1022$ K [12]. As a result, the cooling rate for rods of 1 mm, 1.5 mm and 2 mm in diameter is approximately estimated as 1022 K/s, 454 K/s and 256 K/s, respectively. This indicates that the cooling rate of the as-cast rods is increased with the decrease in the sample diameters, and can be approximately adjusted by producing the cylindrical rods with different diameters.

As seen in Fig. 1, the XRD patterns of the $Al_{86}Si_{0.5}Ni_{4.06}Co_{2.94}Y_6Sc_{0.5}$ alloy rods show that the broad diffraction peak of amorphous feature tends to decline and sharper Bragg peaks appear due to the limited GFA when the diameter of the samples increases from 1 mm to 2 mm. The XRD pattern of the 1-mm-diameter rod exhibits indiscernible crystalline peaks from fcc-Al superimposed on the broad diffuse maxima from the amorphous phase. As reported previously [12], the 1-mm-diameter rod is composed of ~95 vol.% amorphous phase and ~5 vol.% fcc-Al crystalline phase. With the increase in diameter to 1.5 mm and 2 mm for the rod samples, i.e. the decrease of cooling rate during solidification from the melt, crystalline phases including fcc-Al, Al_3Y as well as some unidentified phases precipitated and coarsened according to the full-width at half-maximum for the corresponding crystalline peaks [14].

The transverse cross-sections of the as-cast rods with different diameters were examined by SEM. In Fig. 2(a) and (b), no appreciable contrast revealing the precipitation of a crystalline phase can be seen in the 1-mm-diameter sample. Considering the corresponding XRD results shown above, the featureless contrast in the micron-scale implies the undetectable fcc-Al crystalline phase may exist in the form of submicron-sized particles. More detailed information of the corresponding transmission electron microscopic analysis can be seen in Ref. [12].

As detected from the cross-section of 1.5-mm-diameter sample in Fig. 2(c), an apparently featureless layer with a width of about 200–300 μm appears next to the mold contact surface and wraps the core of the casting. Actually, the ultrafine microstructured layer here is "chill-zone" [15–17], which is formed due to the high crystal nucleation frequency, because the melt in the outer part contacting with the mold would be significantly undercooled. In the inner zone of this sample as shown in Fig. 2(d), different from the chill-zone, dendritic intermetallic phases growing with the interdendritic eutectics phases can be found. According to the EDS analysis, the composition of the dendritic phases (light one) is close to $Al_{68.40}Si_{1.13}Ni_{11.43}Co_{5.92}Y_{12.64}Sc_{0.48}$, i.e. Al-poor intermetallic primary phases precipitated from the hypereutectic melt. The average composition of the ultrafine eutectics is close to $Al_{88.53}Si_{1.06}Ni_{2.68}Co_{2.51}Y_{4.85}Sc_{0.37}$, while their detailed microstructure is hard to be determined.

For the 2-mm-diameter rod, the width of the chill-zone decreases to be about 70 μm, as shown in Fig. 2(e). It is also observed that a few micron/submicron sized particles (white phase) were precipitated in the ultrafine-structured chill-zone. In comparison to the 1.5-mm-diameter rod, the white Al-poor dendritic phase in the inner-zone of the 2-mm-diameter rod is much coarser as shown in Fig. 2(f), and the microstructure of the interdendritic eutectics in the inner-zone can be identified. The network-like Al_3Y-type intermetallic phase (grey one) is coexistent with the ultrafine fcc-Al phase (dark one). These characteristic structures in 2-mm-diameter sample should be resulted from the decreased undercooling and N/G (N is nucleation frequency and G is crystal growth rate) induced by a slower cooling rate compared to those for the 1-mm- and 1.5-mm-diameter rods [17].

The microhardnesses of the samples with different diameters are listed in Table 1. The 1-mm-diameter rod exhibits high microhardness of around 340. The hardness of the edged zone is slightly higher than that of the center zone, which may result from the local heterogeneity of micro/nanoscaled softer fcc-Al crystalline phase embedded in the glassy matrix [12]. The hardness shows a decrease tendency with the decrease in cooing rate for the 1.5-mm- and 2-mm-diameter rods, and mircrohardness of the chill-zones are about 50–80 higher than those of the inner-zones.

Fig. 3 shows compressive stress–strain curves of the rods of 1 mm, 1.5 mm, 2 mm in diameter and the related values are summarized in Table 1. The 1-mm-diameter rod shows yield strength (σ_y: ~1170 MPa) and maximum strength (σ_m: ~1270 MPa), higher in comparison to the other two samples produced at lower cooling rates. The strength shows a stepwise decrease with depressing the cooling rate during the fabrication process. For the alloys of 1.5 mm and 2 mm in diameter, considering the higher hardness of the chill-zones than the inner-zones, the strength would drop relatively when the outer chill-zone region is removed by mechanical grounding, similar to that for the chill zone copper alloys [15]. However, the cooling rate dependence of plasticity is opposite. The plastic strain increases from ~2.4% for the ϕ 1 mm rod to ~4.9% for the ϕ 2 mm rod. As presented in Fig. 4(a), the fracture surface of

Table 1
Vickers microhardness and compressive mechanical properties of the cast alloy rods with different diameters.

Alloy diameter (mm)	Yield strength (MPa)	Maximum strength (MPa)	Plastic strain (%)	Microhardness of edged/inner-zone
1.0	1170	1270	~2.4	347/336
1.5	710	1005	~3.8	234/185
2.0	590	870	~4.9	233/152

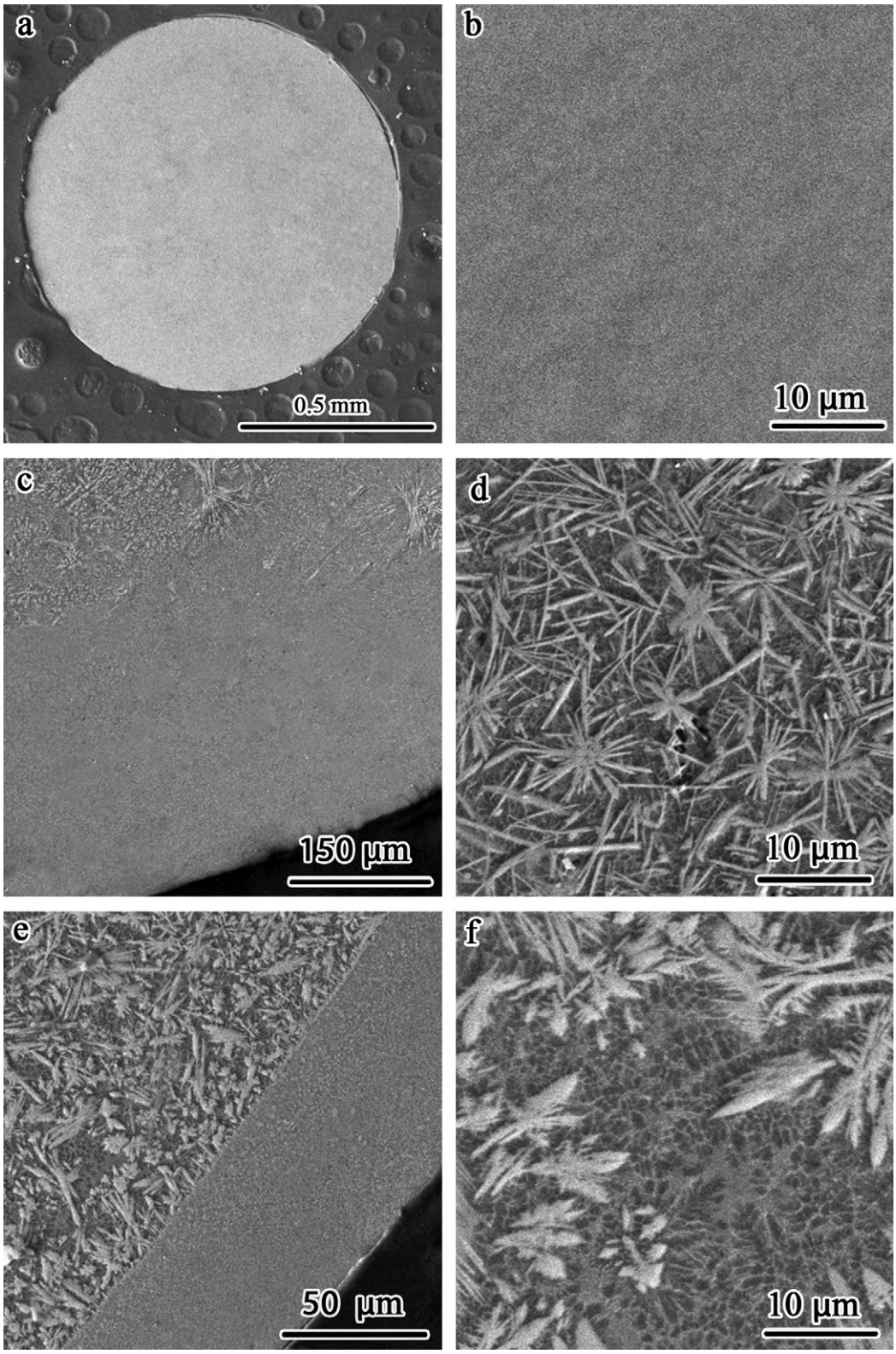

Fig. 2. Backscattering electron images of cross-sections of the cast Al-based rods with a diameter of 1 mm (a) and (b), 1.5 mm (c) and (d), and 2 mm (e) and (f) respectively. (b), (d) and (f) were taken from the rod center part.

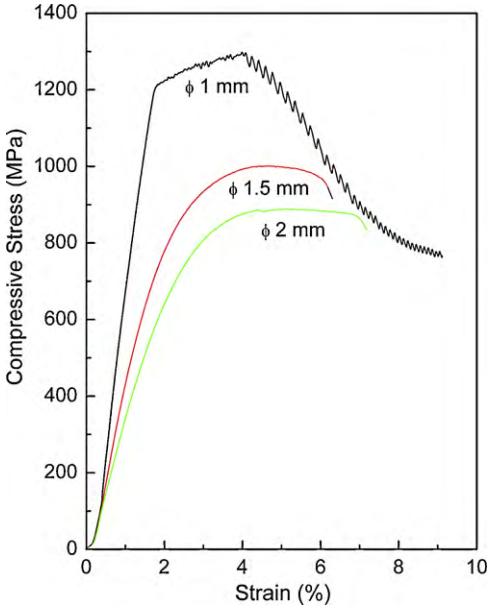

Fig. 3. Compressive stress–strain curves of the Al-based alloy rods with different diameters.

the center of the 1-mm-diameter rod shows a river-like pattern. In comparison, the fracture surface of the rod with larger size is rough and rugged, which may result from the fracture of fcc-Al solid solution phase and intermetallic phases, as shown in Fig. 4(b) and (c).

For the 1-mm-diameter rod, high-density shear bands in multiple directions have been observed [12]. While for the 1.5-mm- and 2-mm-diameter rods, the samples fractured irregularly which deformed in a rather different mechanism. Recently, several models of deformation and fracture mechanism for some rapidly solidified multicomponent alloys have been proposed [15,18–21]. It is well known that the deformation of crystalline alloys is strongly dependent on the dislocation activities and dislocation interactions [22]. The relative work carried out on $Fe_{94}Zr_6$ [23], $Ni_{92}Zr_8$ [24], $Fe_{56}Nb_4Al_{40}$ [25], Ti–Cu–Ni–Sn–Ta [26] ultrafine eutectic composites, etc., reveals that the plastic deformation occurs through a combination of dislocation-based slip in the dendrites and constraint multiple shear banding in the nanostructure eutectic matrix. The composite structure consisting of inner- and chill-zones here provides improved mechanical strength and deformation behavior due to the multiple grain boundaries which act as barriers to dislocations and the coarser internal microstructure [9,17,21]. Furthermore, the morphology of dendritic and eutectic phases controlled by the cooling rate also influences the deformation and fracture behaviors [18,20]. To investigate the initiation and propagation of the crack, the 1.5 mm rod with more distinct chill-zone and inner core compared with the 2 mm rod was taken as a model. The sample subjected to the compression test was unloaded while the nominal plastic strain reached about 1.9%. Then we have observed some cracks already initiated in the chill-zone, as shown in Fig. 5(a). When the 1.5-mm-diameter rod fractured (Fig. 5(b)) finally, a complete crack on the fracture surface can be clearly observed, as shown in Fig. 5(c) and (d). The crack propagated all through the chill-zone, but stopped at the inner-core. Therefore, it can be concluded that the propagation of cracks which are expected to nucleate on the hard surface layer, can be hindered by the presence of multiple dendrites and the soft fcc-Al solid solution phase, leading to the enhanced plasticity of the chill-zone alloys.

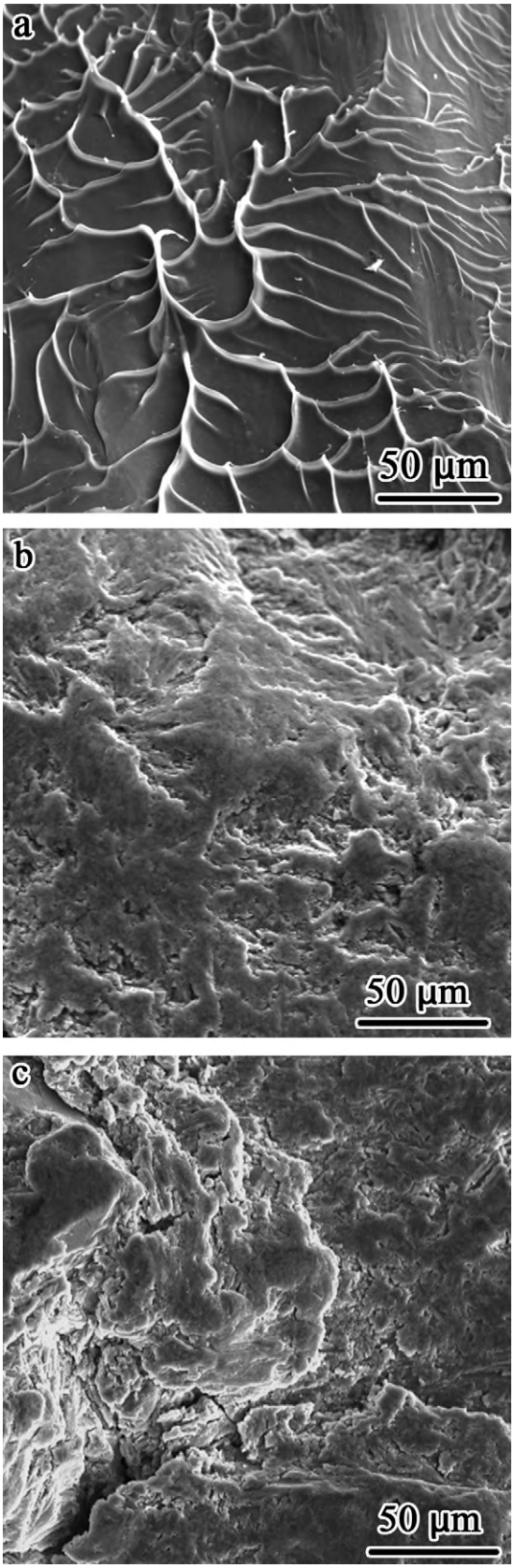

Fig. 4. Typical fracture surfaces of the deformed rods of (a) 1 mm, (b) 1.5 mm and (c) 2 mm in diameters.

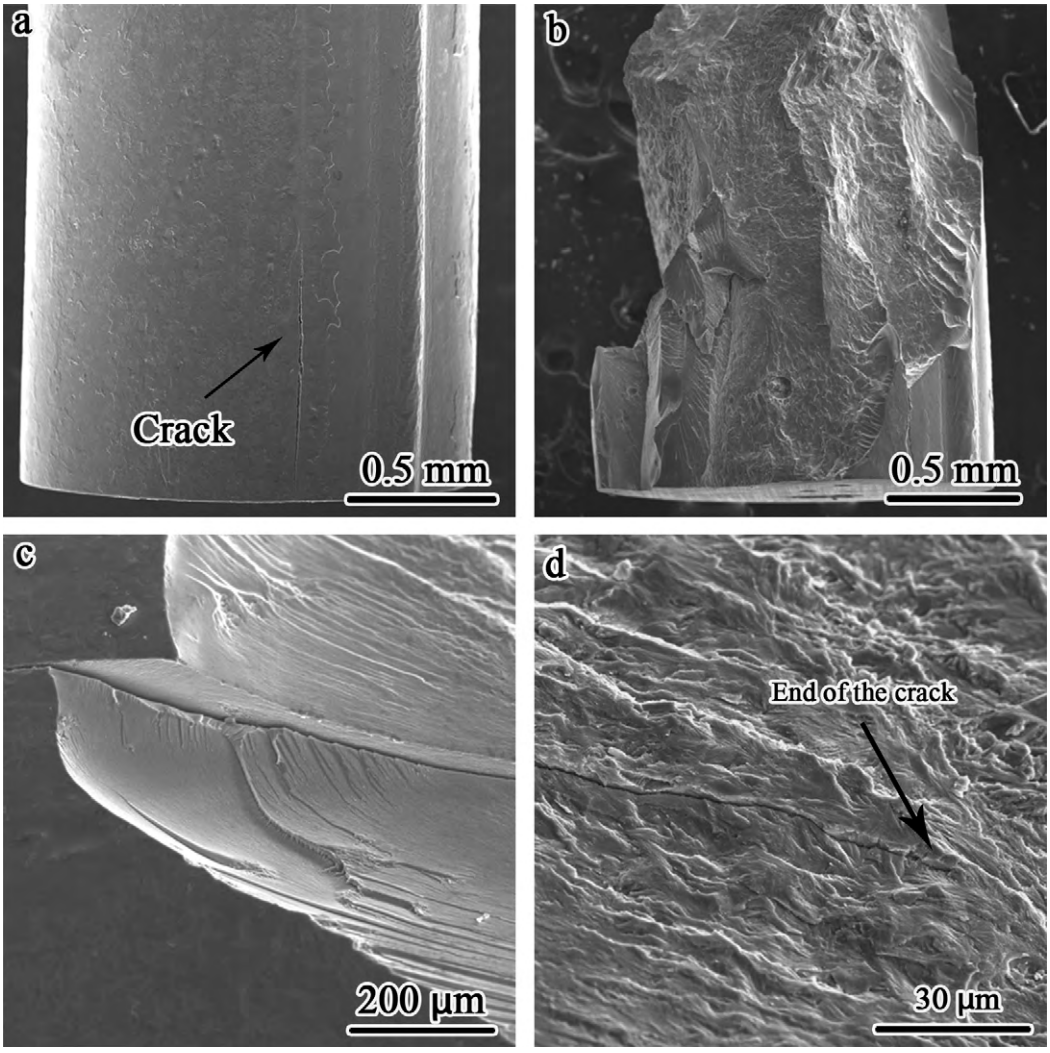

Fig. 5. SEM images of the compressed 1.5-mm-diameter rods. (a) is taken from the rod unloaded at the nominal plastic strain of 1.9%. (b), (c) and (d) show the fracture surface appearance.

4. Conclusions

The compressive mechanical properties, Vickers microhardness and the corresponding microstructure of the Al–Si–Ni–Co–Y–Sc bulk alloys prepared by rapid solidification at different cooling rates were systematically investigated. In comparison to the 1-mm-diameter rod with almost fully amorphous structure, which exhibited compressive strength of 1.27 GPa and plastic strain of 2.4%, the bulk alloys produced at lower cooling rates with chill-zone surface layered structure possess ~1 GPa compressive strength with improved plasticity. It is indicated that by tuning the cooling rates of the glass former during the solidification from the melt, the alloys with a larger size exceeding the critical diameter for glass-formation can possess combined high strength of metallic glasses and large plasticity of conventional crystalline alloys.

Acknowledgements

This research was financially supported by the National Basic Research Program of China (2007CB613900), National Natural Science Foundation of China (Nos. 50631010 and 50771006), and Program for NCET (NCET-07-0041).

References

[1] A.K. Vasudevan, R.D. Roherty, Aluminium Alloys Contemporary Research and Application, San Diego, CA, 1989.
[2] J.R. Davis, Aluminum and Aluminum Alloys, ASM Specialty Handbook, ASM International, 1993.
[3] J.T. Staley, D.J. Lege, J. Phys. IV 3 (1993) 179–190.
[4] S. Scudino, G. Liu, K.G. Prashanth, B. Bartusch, K.B. Surreddi, B.S. Murty, J. Eckert, Acta Mater. 57 (2009) 2029–2039.
[5] Y. He, S.J. Poon, G.J. Shiflet, Science 241 (1988) 1640–1642.
[6] A.P. Tsai, A. Inoue, T. Masumoto, Metall. Trans. 19A (1988) 1369–1370.
[7] A. Inoue, Prog. Mater. Sci. 43 (1998) 365–520.
[8] Z.C. Zhong, X.Y. Jiang, A.L. Greer, Mater. Sci. Eng. A 531 (1997) 226–228.
[9] Y.H. Kim, A. Inoue, T. Masumoto, Mater. Trans. JIM 32 (1991) 559.
[10] W.S. Sanders, J.S. Warner, D.B. Miracle, Intermetallics 14 (2006) 348–351.
[11] B.J. Yang, J.H. Yao, J. Zhang, H.W. Yang, J.Q. Wang, E. Ma, Scripta Mater. 61 (2009) 423–426.
[12] L.C. Zhuo, S.J. Pang, H. Wang, T. Zhang, Chin. Phys. Lett. 26 (2009) 066402.
[13] B. Lohwongwatana, J. Schroers, W.L. Johnson, Phys. Rev. Lett. 96 (2006) 075503.
[14] H.P. Klug, L.E. Alexander, X-ray Diffraction Procedures, Wiley-Interscience, New York, 1974.
[15] A.R. Yavari, K. Ota, K. Georgarakis, A. LeMoulec, F. Charlot, G. Vaughan, A.L. Greer, A. Inoue, Acta Mater. 56 (2008) 1830–1839.
[16] Y. Li, K. Georgarakis, S.J. Pang, J. Antonowicz, F. Charlot, A. LeMoulec, T. Zhang, A.R. Yavari, J. Alloys Compd. 477 (2009) 346–349.
[17] Y. Li, K. Georgarakis, S.J. Pang, T. Zhang, A.R. Yavari, J. Mater. Res. 24 (2009) 1513–1521.
[18] J.M. Park, K.B. Kim, W.T. Kim, D.H. Kim, Appl. Phys. Lett. 91 (2007) 131907.
[19] J.M. Park, N. Mattern, U. Kühn, J. Eckert, K.B. Kim, W.T. Kim, K. Chattopadhyay, D.H. Kim, J. Mater. Res. 24 (2009) 2605–2609.
[20] R. Li, G. Liu, M. Stoica, J. Eckert, Intermetallics 18 (2010) 134.

[21] R. Valiev, Nature 419 (2002) 887–889.
[22] F.R.N. Nabarro, Theory of Crystal Dislocation, Oxford University Press, Oxford, 1967.
[23] J.M. Park, S.W. Sohn, T.E. Kim, K.B. Kim, W.T. Kim, D.H. Kim, Scripta Mater. 57 (2007) 1153.
[24] J.M. Park, T.E. Kim, S.W. Sohn, D.H. Kim, K.B. Kim, W.T. Kim, J. Eckert, Appl. Phys. Lett. 93 (2008) 031903.
[25] J.M. Park, S.W. Sohn, D.H. Kim, K.B. Kim, W.T. Kim, J. Eckert, Appl. Phys. Lett. 92 (2008) 091910.
[26] G. He, W. Löser, J. Eckert, Acta Mater. 51 (2003) 5223–5234.